JPE 13-4-4

http://dx.doi.org/10.6113/JPE.2013.13.4.536

A Study on In-wheel Motor Control to Improve Vehicle Stability Using Human-in-the-Loop Simulation

Sung-Yeon Ko *, Ji-Weon Ko*, Sang-Moon Lee**, Jae-Seung Cheon**, and Hyun-Soo Kim†

†*School of Mechanical Engineering, Sungkyunkwan University, Suwon, Korea
**X-By-Wire Engineering Team, Hyundai Mobis, Yongin, Korea

Abstract

In this study, an integrated motor control algorithm for an in-wheel electric vehicle is suggested. It consists of slip control that controls the in-wheel motor torque using the road friction coefficient and slip ratio; yaw rate control that controls the in-wheel motor torque according to the road friction coefficient and the yaw rate error; and velocity control that controls the vehicle velocity by a weight factor based on the road friction coefficient and the yaw rate error. A co-simulator was developed, which combined the vehicle performance simulator based on MATLAB/Simulink and the vehicle model of CarSim. Based on the co-simulator, a human-in-the-loop simulation environment was constructed, in which a driver can directly control the steering wheel, the accelerator pedal, and the brake pedal in real time. The performance of the integrated motor control algorithm for the in-wheel electric vehicle was evaluated through human-in-the-loop simulations.

Key words: Integrated control, In-wheel, Motor control

I. INTRODUCTION

An in-wheel electric vehicle transmits the power of the motor directly to the wheel. It has higher power transmission efficiency and more available space than the conventional vehicle because it does not have an engine, transmission and axles, which are used in the conventional vehicle [1]. The in-wheel electric vehicle realizes active safety systems as the traction control system (TCS), the anti-lock brake system (ABS), and the electronic stability control (ESC) system by independently controlling the in-wheel motors installed in each wheel [2]. The active safety system of the conventional internal combustion engine vehicle (ICV) was realized by driving power control, which manipulated the engine throttle, fuel injection, or ignition timing, or by braking power control, which manipulated the hydraulic actuator [3]. An in-wheel electric vehicle, however, does not require additional devices such as a hydraulic actuator because it uses in-wheel motors and has a 10 to 100 times faster response than the conventional ICV or a hydraulic actuator [4]. Also, it has better stability than the conventional vehicle because it can apply reverse torques between the left and right wheels by controlling the motors in each wheel [5].

Various studies on in-wheel motor control have been conducted, including the one that controls the wheel slip to satisfy the optimal slip ratio [6], and another one that controls the in-wheel motor using the back electromotive force of the motor that is generated during a slip [7]. Other studies secured turning stability through direct yaw moment control (DYC), in which the in-wheel motors are controlled independently [8-10]; through simultaneous slip control and yaw rate control using a neural network and fuzzy control [11]; through the in-wheel motor speed control using fuzzy control [12]; through a combined motor torque control, in which slip control and yaw rate control are carried out simultaneously based on sliding mode control [13]; and through yaw rate control by estimating the side slip angle [14].

In this study, an integrated motor control algorithm for the in-wheel motor is suggested, which simultaneously considers the slip ratio, yaw rate, vehicle velocity, and road friction to secure vehicle stability. Motor torque is actively controlled by measuring and calculating the slip ratio, yaw rate, and vehicle velocity as well as by estimating the road friction

Manuscript received Jan. 21, 2013; revised Mar. 27, 2013
Recommended for publication by Associate Editor Jin Hur.
†Corresponding Author: hskim@me.skku.ac.kr
Tel: +82-31-290-7438, Fax: +81-31-290-7679, Sungkyunkwan University
*School of Mechanical Engineering, Sungkyunkwan University, Korea

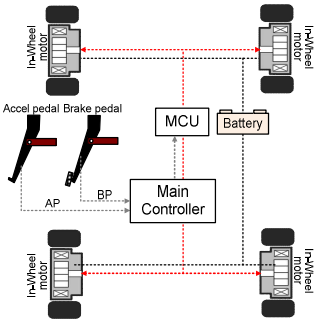

Fig. 1. Structure of the in-wheel electric vehicle.

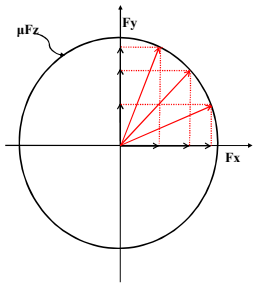

Fig. 2. Friction circle.

characteristics. A co-simulator which combines the vehicle performance simulator based on MATLAB/Simulink and the vehicle model of CarSim is developed to verify the performance of the suggested integrated motor control algorithm. A human-in-the-loop simulation (HILS) environment is constructed based on the co-simulator, and the performance of the integrated motor control for an in-wheel electric vehicle is evaluated.

II. VEHICLE STABILITY CONTROL

Fig. 1 shows the structure of the in-wheel electric vehicle. The accelerator pedal signal or the brake pedal signal generated by the driver is converted to the driving torque or the braking torque of the in-wheel motors in each wheel. In this study, the slip control, yaw rate control, velocity control, and integrated motor control of the in-wheel electric vehicle are suggested to improve the vehicle stability.

A. Slip Control

Fig. 2 shows a friction circle. In the friction circle, the vector sum of the lateral force and the longitudinal force must be equal to or less than the product of the normal force and the road friction coefficient, which is summarized as follows:

$$\mu F_z \geq \sqrt{F_x{}^2 + F_y{}^2} \tag{1}$$

where μ is the road friction coefficient; F_z, the normal force on a wheel; F_x, the longitudinal force; and F_y, the lateral force. During actual driving, however, a driving or braking force larger than that in the friction circle can be generated. In this case, only the force that corresponds to the friction circle is transmitted to the road, and the remaining force spins the wheels. To prevent the generation of a driving or braking force larger than that in the friction circle, Equation (1) is converted to the following driving force limit equation:

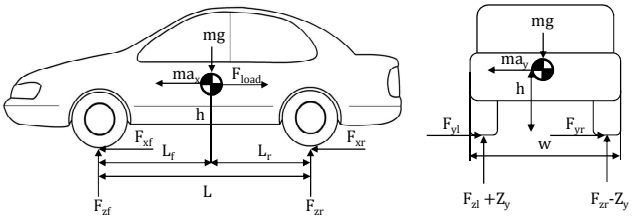

(a) Longitudinal direction (b) Lateral direction

Fig. 3. Vehicle model.

$$F_{x\_\text{limit}} = \sqrt{(\mu F_{z\_cal})^2 - F_{y\_cal}{}^2} \tag{2}$$

where F_{x_limit} is the driving force limit; F_{z_cal}, the calculated normal force; and F_{y_cal}, the calculated lateral force. In other words, the driving force limit can be obtained when the road friction coefficient, the normal force, and the lateral force are known.

Since the road friction coefficient cannot be measured during driving, various estimation methods have been suggested. They include the method of using the linear gradient of the vertical force according to the slip ratio per friction coefficient [15], the method of using the non-linear tire model [16], the method that considers the load movement using a vehicle model [17], and the method based on sensor signals and dynamic equations [18], among others. The last method [18] was used in this study.

Fig. 3 shows a vehicle model for calculating the normal force (F_{z_cal}) applied to a vehicle. Considering the external forces in the vertical and longitudinal directions on a vehicle, the normal force on each wheel can be derived as follows:

$$\begin{aligned}
F_{zfl_cal} &= \frac{h(ma_x - F_{load}) + L_r mg}{L} + \frac{hma_y}{w} \\
F_{zfr_cal} &= \frac{h(ma_x - F_{load}) + L_r mg}{L} - \frac{hma_y}{w} \\
F_{zrl_cal} &= \frac{-h(ma_x - F_{load}) + L_f mg}{L} + \frac{hma_y}{w} \\
F_{zrr_cal} &= \frac{-h(ma_x - F_{load}) + L_f mg}{L} - \frac{hma_y}{w}
\end{aligned} \tag{3}$$

where F_{zfl_cal} is the normal force on the front left wheel; F_{zfr_cal}, the normal force on the front right wheel; F_{zrl_cal}, the normal force on the rear left wheel; F_{zrr_cal}, the normal force on the rear right wheel; h, the height of the vehicle from the center of gravity; m, the vehicle mass; g, the acceleration of gravity; a_x, the longitudinal acceleration; a_y, the lateral acceleration; F_{load},

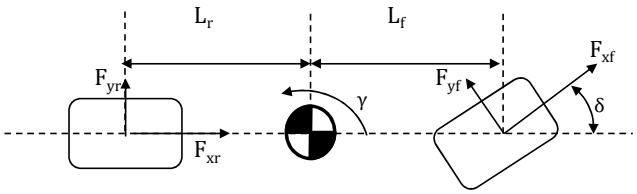

Fig. 4. Two-wheel vehicle model.

the driving resistance; L_f, the longitudinal distance between the center of gravity and the front wheel centerline; L_r, the longitudinal distance between the center of gravity and the rear wheel centerline; L, the longitudinal distance between the front wheel centerline and the rear wheel centerline; and w, the track width.

Next, the lateral force (F_{y_cal}) on the vehicle needs to be obtained. Fig. 4 shows a two-wheel model of the vehicle. From the two-wheel model, the dynamic equations of vehicle motion can be derived:

$$I\dot{\gamma} = L_f F_{xf}\sin\delta + L_f F_{yf}\cos\delta - L_r F_{yr}$$
$$ma_y = F_{xf}\sin\delta + F_{yf}\cos\delta + F_{yr} \quad (4)$$

where I is the moment of inertia; γ, the yaw rate; F_{xf}, the longitudinal force on the front wheel; F_{xr}, the longitudinal force on the real wheel; F_{yf}, the lateral force on the front wheel; F_{yr}, the lateral force on the rear wheel; and δ, the steering wheel angle. Assuming that $F_{xf} = 0$ and $F_{xr} = 0$, the lateral forces on the front and rear wheels can be calculated as follows:

$$F_{yf\_cal} = \frac{I\dot{\gamma} + ma_y L_r}{L\cos\delta}$$
$$F_{yr\_cal} = \frac{-I\dot{\gamma} + ma_y L_f}{L} \quad (5)$$

where F_{yf_cal} is the lateral force on the front wheel and F_{yr_cal}, the lateral force on the real wheel. The lateral force on each wheel can be calculated using the normal forces from Equation (3) and the lateral forces on the front and rear wheels from Equation (5), as follows [19]:

$$F_{yfl\_cal} = F_{yf\_cal}\frac{F_{zfl\_cal}}{F_{zfl\_cal} + F_{zfr\_cal}}$$
$$F_{yfr\_cal} = F_{yf\_cal}\frac{F_{zfr\_cal}}{F_{zfl\_cal} + F_{zfr\_cal}}$$
$$F_{yrl\_cal} = F_{yr\_cal}\frac{F_{zrl\_cal}}{F_{zrl\_cal} + F_{zrr\_cal}} \quad (6)$$
$$F_{yrr\_cal} = F_{yr\_cal}\frac{F_{zrr\_cal}}{F_{zrl\_cal} + F_{zrr\_cal}}$$

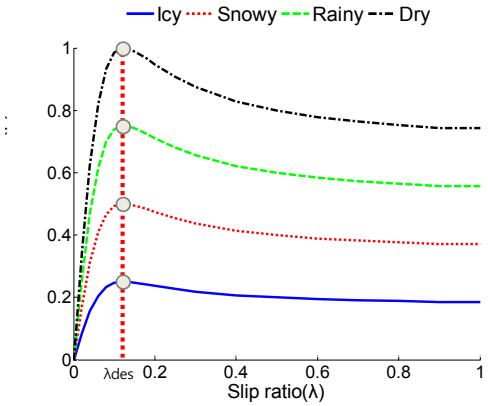

Fig. 5. Non-linear tire model (slip ratio vs friction coefficient).

where F_{yfl_cal} is the lateral force on the front left wheel; F_{yfr_cal}, the lateral force on the front right wheel; F_{yrl_cal}, the lateral force on the rear left wheel; and F_{yrr_cal}, the lateral force on the rear right wheel. After determining the driving force limit F_{x_limit} (Equation (2)) from Equations (3)-(6), the in-wheel motor torque limit can be obtained as follows:

$$T_{\text{limit}} = RF_{x\_\text{limit}} = R\sqrt{(\mu F_{z\_cal})^2 - F_{y\_cal}{}^2} \quad (7)$$

where R is the tire radius.

The motor torque control using only the friction circle, however, cannot guarantee vehicle stability in various driving conditions (such as sudden acceleration, braking, or turning on a low-friction road) due to the errors in the estimations of the road friction coefficient, normal force, and lateral force. For improved control performance, a feedback control based on the slip ratio was added. The following equation represents the motor torque limit with the added feedback control:

$$T_{\text{limit}} = RF_{x\_\text{limit}} + K_{slip\ control}(\lambda_{des} - \lambda_{cal})\times(\lambda_{cal} > \lambda_{des}) \quad (8)$$

where $K_{\text{slip control}}$ is the P control gain; λ_{des}, the desired slip ratio; and λ_{cal}, the calculated slip ratio. The desired slip ratio (λ_{des}) is the slip ratio at the condition of maximum friction coefficient in the non-linear tire model in Fig. 5. The calculated slip ratio (λ_{cal}) can be obtained by the following equations:

$$\lambda_{cal} = \frac{R\omega - V}{R\omega} \quad at\ acceleration\ region$$
$$\lambda_{cal} = \frac{V - R\omega}{V} \quad at\ deceleration\ region \quad (9)$$

where V is the vehicle velocity and ω, the wheel velocity. The feedback control element $K_{\text{slip control}}(\lambda_{des} - \lambda_{cal})$ for the motor torque limit was applied only when λ_{cal} exceeded λ_{des}.

B. Yaw Rate Control

Fig. 6 shows a block diagram of the yaw rate control. After the vehicle state is determined using $\gamma_{desired}$ and γ_{sensor}, the yaw

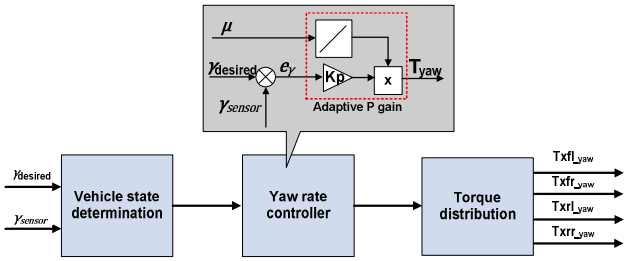

Fig. 6. Block diagram of the yaw rate control.

rate torque T_{yaw} is obtained by multiplying the yaw rate error e_γ with the adaptive P gain. The desired yaw rate can be obtained as follows:

$$\gamma_{desired} = \frac{V}{L + (\frac{W_f}{C_f} - \frac{W_r}{C_r})\frac{V^2}{g}}\delta \quad (10)$$

where $\gamma_{desired}$ is the desired yaw rate; C_f, the cornering stiffness of the front wheels; C_r, the cornering stiffness of the rear wheels; W_f, the normal load on the front wheels; and W_r, the normal load on the rear wheels.

Since a vehicle easily spins at a little yaw moment on a low-friction road, and hardly spins at a large yaw moment on a high-friction road, an adaptive P controller is designed based on these characteristics so that the control gain increases with the increase of the road friction coefficient. The suggested yaw rate torque that directly generates the yaw moment is obtained as follows:

$$T_{yaw} = (a\mu + b) \times K_{Pyaw\ rate\ control} \times (\gamma_{desired} - \gamma_{sensor}) \quad (11)$$

where $(a\mu+b)K_{Pyaw\ rate\ control}$ is the adaptive P gain and γ_{sensor} is the measured yaw rate. $a\mu+b$ in the adaptive P gain is designed to increase linearly with increases in the road friction coefficient. A linear function is designed since the force that can be applied to a tire is linearly proportional to the road friction coefficient. This T_{yaw} is distributed to the left and right wheels in opposite directions depending on the vehicle's state (understeered or oversteered). It generates a direct yaw moment and improves the vehicle's turning performance.

C. Velocity Control

Velocity control determines the velocity at which the vehicle can safely turn. It controls the vehicle velocity and helps the vehicle to make a safe turn when the vehicle velocity exceeds the velocity limit. In the case of a circular turn, the turning radius can be estimated by dividing the vehicle velocity by the yaw rate measured with sensor:

$$\rho = \frac{V}{\gamma} = \frac{V}{\gamma_{sensor}} \quad (12)$$

where ρ is the turning radius. Using this turning radius, the vehicle velocity limit for turning is suggested as follows:

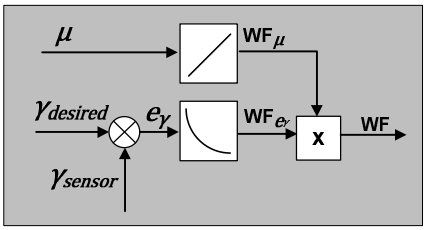

Fig. 7. Weight factor (WF).

$$V_{\text{limit}} = WF \times \rho \times \gamma_{desired} \quad (13)$$

where V_{limit} is the vehicle velocity limit and WF is the weight factor.

Fig. 7 shows the suggested WF diagram. The WF is designed considering the road friction coefficient and the yaw rate error.

The weight factor WF_μ according to the road friction coefficient is obtained as follows:

$$WF_\mu = f(\mu) = c\mu + d \quad (14)$$

WF_μ is designed to increase linearly. A linear function is designed since the force that can be applied to a tire is linearly proportional to the road friction coefficient.

The weight factor WFe_γ according to the yaw rate error is designed as follows:

$$WFe_\gamma = f(e_\gamma) = a'e_\gamma^{\,2} + b'e_\gamma + c' \quad (15)$$

A quadratic function of WFe_γ is designed to reduce the vehicle velocity limit of Equation (13) by rapidly reducing WF when the yaw rate error rapidly increases. WF is obtained by multiplying WF_μ with WFe_γ, as follows:

$$WF = WF_\mu \times WFe_\gamma \quad (16)$$

The following equation determines the execution of velocity control by comparing the vehicle velocity and the vehicle velocity limit, as follows:

$$V_{\text{limit signal}} = \begin{cases} V - V_{\text{limit}} < V_{\text{set}} & \cdots 0\ (stable\ \ state) \\ V - V_{\text{limit}} \geq V_{\text{set}} & \cdots 1\ (unstable\ \ state) \end{cases} \quad (17)$$

where $V_{limit\ signal}$ is a signal that judges the execution of the velocity control during turning, and V_{set}, the vehicle velocity setting value that is selected to distinguish a stable state from an unstable state. The vehicle velocity setting value (V_{set}) is selected as the difference between the velocity (V) and the velocity limit (V_{limit}), at which the vehicle's state becomes unstable in simulations. A vehicle is judged stable when the difference between V and V_{limit} is under V_{set}, and unstable when over V_{set}. When the vehicle state is determined to be unstable, the following velocity control according to the velocity limit is performed after the accelerator pedal position (AP) is lifted up to 0 regardless of the driver's demand:

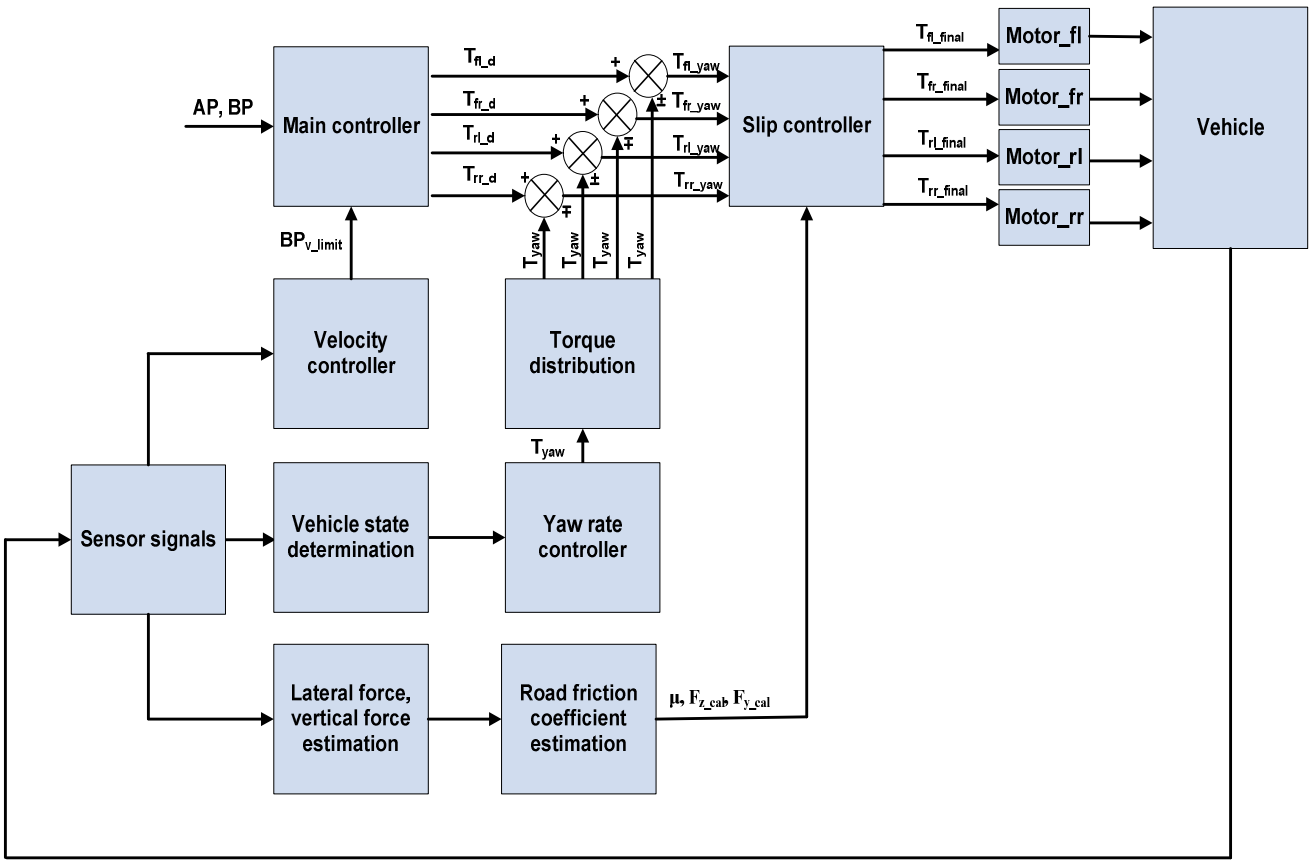

Fig. 8. Block diagram of the integrated motor control.

$$BP_{\text{V\_limit}} = K_{Pvelocity\ control}(V - V_{\text{limit}}) + K_{Ivelocity\ control}\int (V - V_{\text{limit}})dt,\ when\ V_{\text{limit signal}} : 1 \quad (18)$$

where BP_{V_limit} is a signal that controls the brake pedal position (BP); $K_{Pvelocity\ control}$, the P control gain; and $K_{Ivelocity\ control}$, the I control gain. BP_{V_limit} is input to the main controller under an unstable state ($V_{limit\ signal}$ = 1), which is converted to a braking force that drops the vehicle velocity below the velocity limit.

III. Integrated Motor Control

Fig. 8 shows the block diagram of the integrated motor control algorithm. The driver's manipulation of the accelerator pedal or the brake pedal is converted to accelerator pedal position (AP) or brake pedal position (BP) signal, which is transferred to the main controller. At this time, the velocity controller inputs the $V_{limit\ signal}$ and the BP_{V_limit} into the main controller according to the vehicle state. The main controller judges the vehicle state for the input $V_{limit\ signal}$, and converts the AP, BP, and BP_{V_limit} signals into motor torques for each wheel. The yaw rate controller adds T_{yaw} to these motor torques depending on the vehicle state (understeered or oversteered), and the sums are input to the slip controller.

The slip controller finally controls the motor torque after comparing the motor torque limit of Equation (7) and the input torque. The final in-wheel motor torques are as follows:

$$T_{fl\_final} = \begin{cases} T_{fl\_d}(AP, BP, BP_{V\_\text{limit}}) \pm T_{yaw} & (T_{fl\_final} < T_{fl\_\text{limit}}) \\ T_{fl\_\text{limit}} & (T_{fl\_final} \geq T_{fl\_\text{limit}}) \end{cases}$$

$$T_{fr\_final} = \begin{cases} T_{fr\_d}(AP, BP, BP_{V\_\text{limit}}) \mp T_{yaw} & (T_{fr\_final} < T_{fr\_\text{limit}}) \\ T_{fr\_\text{limit}} & (T_{fr\_final} \geq T_{fr\_\text{limit}}) \end{cases} \quad (19)$$

$$T_{rl\_final} = \begin{cases} T_{rl\_d}(AP, BP, BP_{V\_\text{limit}}) \pm T_{yaw} & (T_{rl\_final} < T_{rl\_\text{limit}}) \\ T_{rl\_\text{limit}} & (T_{rl\_final} \geq T_{rl\_\text{limit}}) \end{cases}$$

$$T_{rr\_final} = \begin{cases} T_{rr\_d}(AP, BP, BP_{V\_\text{limit}}) \mp T_{yaw} & (T_{rr\_final} < T_{rr\_\text{limit}}) \\ T_{rr\_\text{limit}} & (T_{rr\_final} \geq T_{rr\_\text{limit}}) \end{cases}$$

IV. Human-in-the-Loop Simulation for the Integrated Motor Control

The human-in-the-loop simulator (Fig. 9) was developed to evaluate the performance of the integrated motor control algorithm suggested in this study. Since the driver can directly drive in an environment similar to the actual one in HILS, HILS can evaluate the performance of the control logic while minimizing the driver's effect on the controller. HILS is

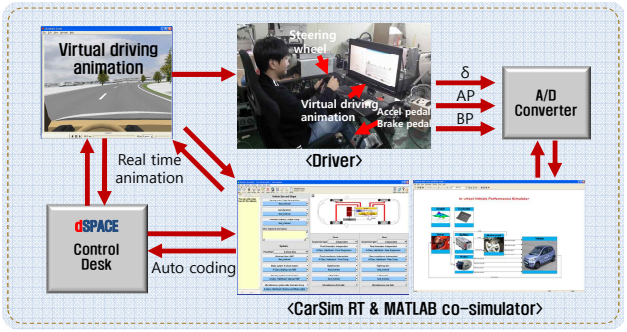

Fig. 9. Human-in-the-loop simulator (HILS).

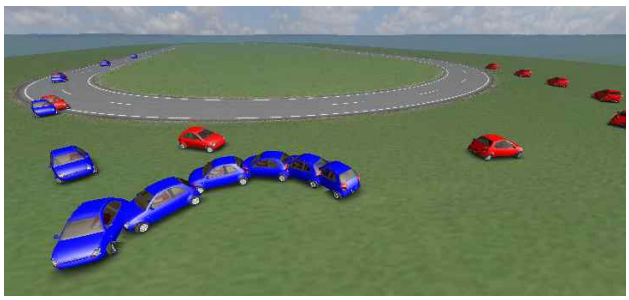

Fig. 10. Animation of the vehicle trajectory.

performed as follows. When the driver directly manipulates the steering wheel, accelerator pedal and brake pedal, these manipulation signals go to the co-simulator, which is composed of CarSim RT and MATLAB/Simulink. CarSim RT, in connection with dSPACE Control Desk, displays vehicle driving animation in real time, and the driver manipulates the steering wheel, accelerator pedal and brake pedal, watching this animation.

Fig. 10 shows the vehicle trajectory seen in the CarSim software animation for no control and integrated motor control after HILS performance.

The vehicle parameters are given in Table I.

V. Human-in-the-Loop Simulation Results

HILS was conducted to evaluate the performance of the suggested integrated motor control algorithm for an in-wheel electric vehicle.

A. J-turn Test

The J-turn test conditions are as follows.

- Initial velocity: 80 kph
- Maintain velocity of 80 kph for 0-15 sec and brake fully after 15 sec (driver control)
- Steering wheel angle at 0 degrees for 0-5 sec and at 200 degrees after 5 sec (driver control)
- Road friction coefficient: $\mu = 0.85$

TABLE I

Vehicle Parameters

Parameter		Value	Unit
Vehicle	Sprung mass	1,200	Kg
	Distance between the C.G. of the sprung mass and the front wheel centerline	1,103	mm
	Distance between the C.G. of the sprung mass and the rear wheel centerline	1,244	mm
	Distance between the front wheel centerline and the rear wheel centerline	2,347	mm
	Vehicle height from the C.G.	540	mm
	Track width	1,595	mm
	Roll inertia	288	Kgm^2
	Pitch inertia	1,111	Kgm^2
	Yaw inertia	1,111	Kgm^2
	Effective tire rolling radius	273.6	mm
	Frontal area	1.9	m^2
In-wheel motor	Power	16	kW
	Maximum torque	123.2	Nm
	Maximum speed	5,000	rpm
	Reduction gear ratio	4	-
Battery	Nominal voltage	270	V
	Capacity	12	Ah

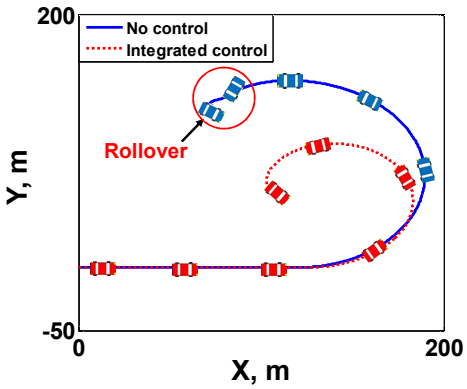

Fig. 11. J-turn vehicle trajectory.

Fig. 11 shows a vehicle trajectory obtained from the J-turn HILS. With no control, the turn had a larger radius. Full braking after 15 sec yielded a rollover. On the contrary, the integrated motor control resulted in a turn with a smaller radius and a safe stop with full braking after 15 sec.

Fig. 12 shows the J-turn simulation results. With no control, maximum torque was generated (c and d) after full braking at t

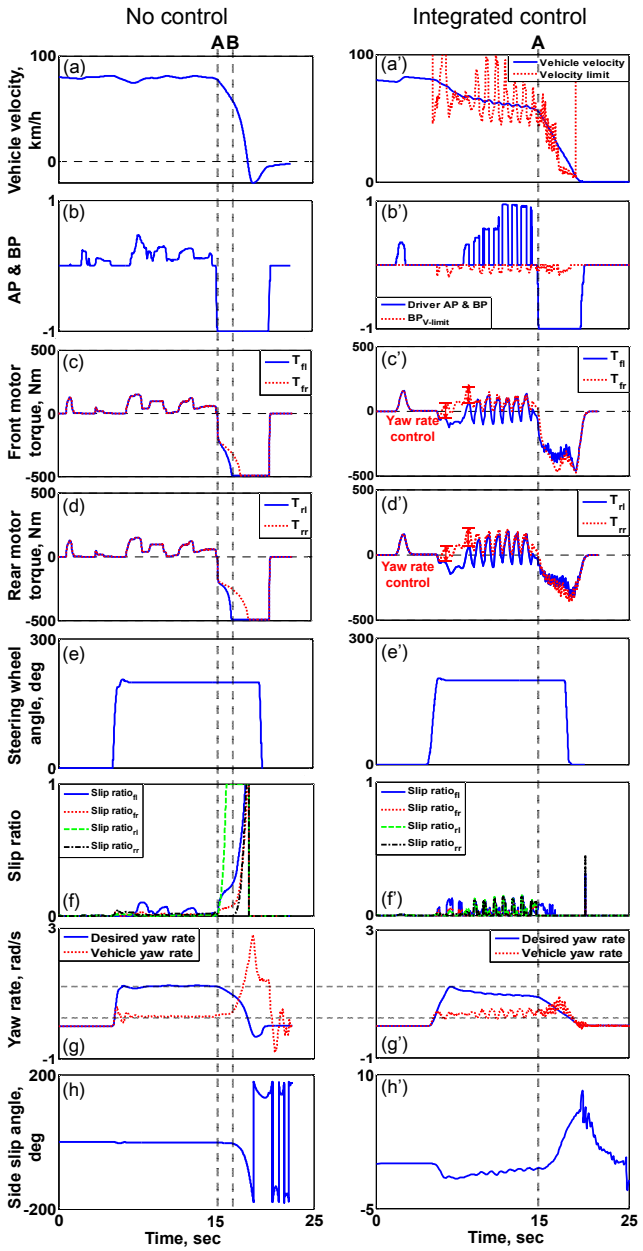

Fig. 12. J-turn results.

= 15 sec, which caused the slip ratio to increase fast after point A and to reach 1 (f). Also, the sudden increases in the yaw rate (g) and the side slip angle (h) yielded a rollover after point B. Different motor braking torques were generated for the left and right wheels during the braking period (c and d). This was because the slip ratio of the left wheel increased faster than that of the right wheel (f), and the left wheel speed was reduced earlier than the right, which led to the application of a larger braking torque on the left wheel due to the motor characteristics. With the integrated motor control, when the vehicle velocity exceeded the velocity limit (a'), the AP input dropped to 0 regardless of the driver's demand, the BP_{V_limit} was applied, and the velocity decreased (b') due to the velocity control. While the driver stepped more on the accelerator pedal (b') to maintain the driving condition of 80 kph, the vehicle velocity was controlled by the velocity control (a'). Driving torque was generated by the AP input, and braking torque, by the BP_{V_limit} (c' and d'). Also, different motor torques were applied for the left and right wheels by the yaw rate control (c' and d'). They improved the vehicle's turning performance by generating a direct yaw moment to the vehicle. After a full brake at t = 15sec (point A), the motor torques of the integrated motor control were smaller than those of no control (c, d, c' and d') because the motor torque was limited by the slip control. A lower slip ratio was generated (f'), and the errors in the desired yaw rate and the vehicle yaw rate were lower than those of no control (g and g'). Also, a smaller side slip angle was generated (h').

In conclusion, without control, a rollover occurred, but with the integrated motor control, a smaller turning radius, lower slip ratio, and reduced yaw rate error and side slip angle were obtained.

B. U-turn Test

The U-turn test conditions are as follows.

- Initial velocity: 70kph
- Maintain 70kph before turning
- Control the steering wheel while watching the target path in real time (driver control)
- If the driver feels a slip of the vehicle in the lateral direction, he performs emergency braking (driver control)
- Target path: 200m straight, Oval: 50m radius
- Road friction coefficient: μ=0.5

Fig. 13 shows the U-turn vehicle trajectory. With no control, the turn resulted in a lateral vehicle slip, emergency braking, and a rollover. With the integrated motor control, the vehicle followed the target path, showing a small deviation.

Fig. 14 shows the HILS results for the U-turn. In the case of no control, the driver started turning at point A and increased the steering wheel angle, but could not follow the target path, so driver had to increase the steering wheel angle up to 380 degrees (e). Also, the driver performed emergency braking as the vehicle slipped in the lateral direction at point B. A 480Nm motor torque was generated in the negative direction (c and d), and the slip ratio reached 1 (f). The sudden increases in the yaw rate (g) and the side slip angle (h) after point C yielded a rollover. Different motor braking torques were generated for the front and rear wheels in the braking period after point B (c and d). This was because the slip ratio of the front wheel increased fast, and the front wheel speed decreased earlier than the rear wheel speed (f), so the front braking torques increased fast due to the motor characteristics.

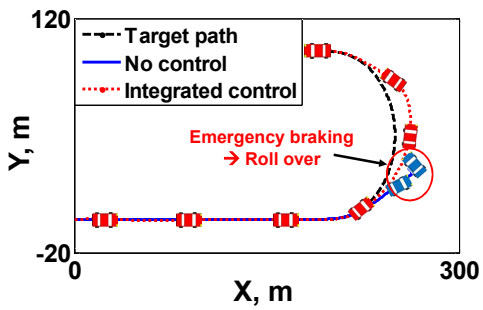

Fig. 13. U-turn vehicle trajectory.

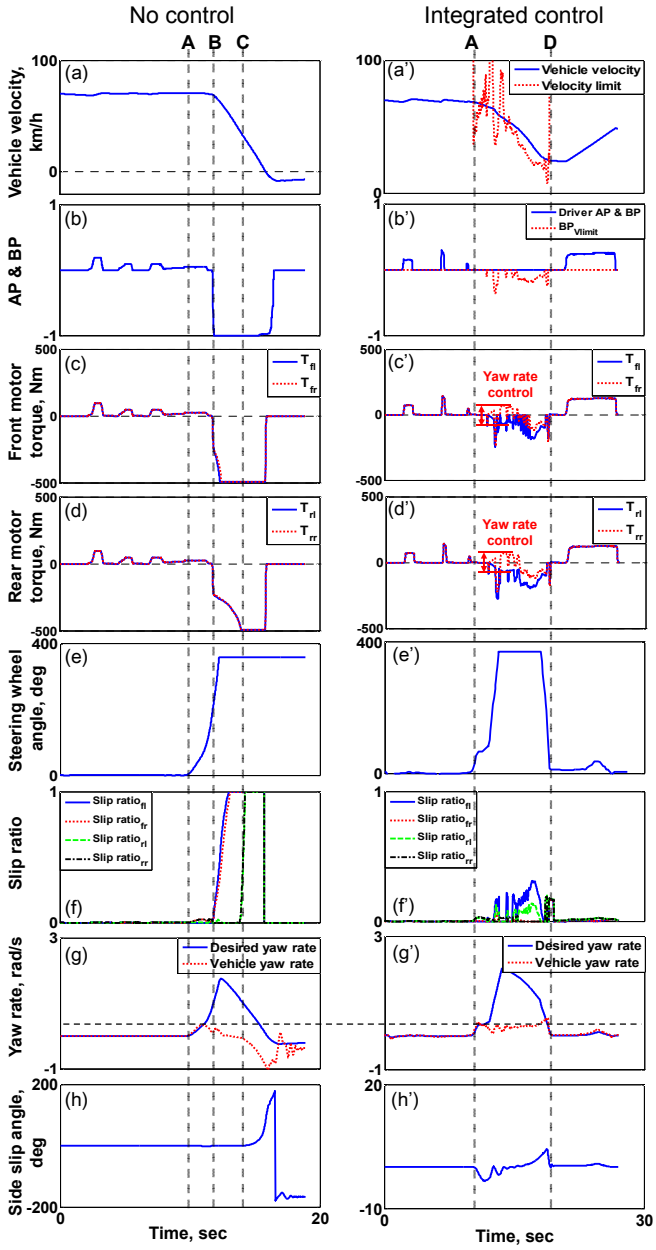

Fig. 14. U-turn results.

In the case of the integrated motor control, the driver started turning at point A and increased the steering wheel angle up to 380 degrees to follow the target path (e'). When the vehicle velocity exceeded the velocity limit (a'), the velocity control applied BP_{V_limit} regardless of the driver's demand (b'), and the velocity decreased due to the braking torque (a'). Also, different motor torque inputs for the left and right wheels in the yaw rate control generated a direct yaw moment and improved the vehicle's turning performance (c' and d'). A lower slip ratio was generated in the braking path (f'). In terms of the yaw rate, the desired yaw rate was similar to that in the case of no control, but the vehicle yaw rate was kept at a constant level (g and g'). This meant that the vehicle turned with a constant radius. The driver manipulated the steering wheel angle back to 0 at the end of the U-turn (point D) (e'), and then accelerated the vehicle by stepping on the accelerator pedal (b').

In conclusion, for no control, the driver felt the slip of the vehicle in the lateral direction and consequently, stepped on the emergency brake after point B, but a rollover ultimately occurred. In contrast, with the integrated motor control, the vehicle safely turned with the motor torque control after the driver started turning at point A. The driver re-accelerated the vehicle at the end of the U-turn (point D).

The HILS results showed that for the J-turn with the road friction coefficient $\mu = 0.85$, with the integrated motor control, the driver made a turn with a smaller radius and the slip ratio, yaw rate error, and side slip angle were smaller than those with no control. With the integrated motor control, braking was carried out safely, whereas with no control, a rollover occurred. For the U-turn with $\mu = 0.5$, with the integrated motor control, the driver followed a path similar to the target path, and the slip ratio, yaw rate error, and side slip angle were small. With no control, the driver performed emergency braking as the vehicle slipped in the lateral direction, causing the vehicle to rollover. The integrated motor control algorithm suggested in this study for the in-wheel electric vehicle improved the vehicle stability.

VI. Conclusion

An integrated motor control algorithm that controls the torque of each motor was suggested to improve the turning stability of in-wheel electric vehicles. The integrated motor control consisted of slip control, yaw rate control, and velocity control. Slip control prevented slips by controlling the in-wheel motor torque of each wheel according to the road friction coefficient and the slip ratio. Yaw rate control improved the vehicle turning performance by generating a direct yaw moment through the independent operation of each in-wheel motor. Velocity control controlled the vehicle velocity by using the weight factor based on the road friction coefficient and the yaw rate error and enhanced the vehicle turning performance. Each control actively controlled the motor torque according to the road friction characteristics. A HILS environment was developed in which a driver directly manipulated the steering wheel, accelerator pedal, and brake pedal in real time to verify

the performance of the integrated motor control. The performance of the integrated motor control was evaluated both for a J-turn on a road with a road friction coefficient of μ=0.85 and for a U-turn on a road of μ=0.5. In the integrated motor control, a smaller turning radius and a lower yaw rate error than those of no control were observed for both the J-turn and U-turn driving tests. The integrated motor control showed safe turning and braking performance at a low slip ratio, yaw rate, and side slip angle, whereas no control resulted in a rollover with sudden increases in the slip ratio, yaw rate, and side slip angle. Accordingly, vehicle stability was improved by the integrated motor control suggested in this study.

ACKNOWLEDGMENT

This work was supported by Advanced System Integration Team of Hyundai Mobis and the Technology Innovation Program funded by the Ministry of Knowledge Economy (MKE, Korea).

REFERENCES

[1] T. Lee and D. Kim, "Technical Trend of In-Wheel System," *KSAE Journal of the Korean Society of Automotive Engineers*, Vol. 31, No. 4, pp. 21-25, 2009.

[2] S. Kim, J. Jeom, and J. Cheon, "The Future of Brake Systems," *KSAE Journal of the Korean Society of Automotive Engineers*, Vol. 26 No. 5 (WN.132), pp. 3-10, 2004.

[3] J. Song, H. Kim, and B. Kim, "Vehicle longitudinal and lateral stability enhancement using a TCS and yaw motion controller," *International Journal of Automotive Technology*, Vol. 8, No. 1, pp. 49-57, 2007.

[4] Y. Hori, "Future vehicle driven by electricity and control-research on four-wheel-motored 'UOT electric march II'," *IEEE Trans. Ind. Electron*., Vol. 51, No. 5, pp. 954–962, Oct. 2004.

[5] S. Sakai, H. Sado, and Y. Hori "Motion control in an electric vehicle with 4-independently driven in-wheel motors," *IEEE/ASME Trans. Mechatron.*, Vol. 4, No.1, pp. 9-16, Mar. 1999.

[6] Y. Hori, Y. Toyoda, and Y. Tsuruoka, "Traction control of electric vehicle : basic experimental results using the test EV 'UOT Electric March'," *IEEE Trans. Ind. Appl*., Vol. 34, No. 5, pp. 1131–1138, Sep./Oct. 1998.

[7] X. Liu, L. Li, and Y. Hori, "Optimal traction control for ev utilizing fast torque response of electric motor," *Industrial Electronics Society, 2005. IECON 2005. 31st Annual Conference of IEEE*, pp. 2614-2619, 2005.

[8] M. Kamachi and K. Walters, "A research of Direct Yaw-Moment Control on Slippery road for in-wheel motor vehicle," *EVS22*, pp. 2122–-2133, 2006.

[9] S. Sakai, H. Sado, and Y. Hori, "Motion control in an electric vehicle with four independently driven in-wheel motors," *IEEE/ASME Trans. Mechatron*., Vol. 4, No. 1, pp. 9–16, Mar. 1999.

[10] D. Kim, S. Hwang, and H. Kim, "Vehicle stability enhancement of four-wheel-drive hybrid electric vehicle using rear motor control," *IEEE Trans. Veh. Technol.*, Vol. 57, No. 2, pp. 727-735, Mar. 2008.

[11] F. Tahami, R. Kazemi, and S. Farhanghi, "A novel driver assist stablity system for all-wheel-drive electric vehicles," *IEEE Trans. Veh. Technol*., Vol. 52, No. 3, pp. 682-692, May 2003.

[12] A. Nasri, A. Hazzab, and I.K Bousserhane, "Fuzzy logic speed control stability improvement of lightweight electric vehicle drive," *Journal of Electrical Engineering & Technology*, Vol. 5, No. 1, pp. 129-139, Jan. 2010.

[13] J. Kim, C. Park, S. Hwang, Y. Hori, and H. Kim, "Control algorithm for an independent motor-drive vehicle," *IEEE Trans. Veh. Technol.*, Vol. 59, No. 7, pp. 3213-3222, Sep. 2010.

[14] C. Geng, L. Mostefai, M. Denai, and Y. Hori, "Direct yaw-moment control of an in-wheel_motored electric vehicle based on body slip angle fuzzy observer," *IEEE Trans. Ind. Electron.*, Vol. 56, No. 5, pp. 1411-1419, May 2009.

[15] Y. Nakao, H. Kawasaki, and D. J.Major, "Estimation of friction levels between tire and road," *SAE World Congress Detroit*, 2002.

[16] J. Wang, L. Alexander, and R. Rajamani, "Friction estimation on highway vehicles using longitudinal measurements," *Journal of Dynamic, Measurement, and Control*, Vol. 126, 2004.

[17] J. Lee, S. Jung, S. Heo, H. Choi, H. Kim, K. Noh, I. Park, and J. Kim, "Improvement of road friction estimation using full vehicle model," KSAE10-B0128, 2010.

[18] S. Ko, J. Ko, J. Kim, S. Lee, J. Cheon, and H. Kim, "Development of road friction estimation and TCS control algorithm for in-wheel independent drive vehicle," KSAE11-A0172, 2011.

[19] N. Mutoh, O. Nishida, and T. Takayanagi, "Driving torque distribution method for front-and-rear-wheel-independent-drive-type electric vehicles (FRID EVs) at the time of cornering," EVS-25, 2010.

Sung-Yeon Ko received B.S and M.S in mechanical engineering from Sungkyunkwan University, Suwon, Korea, in 2010 and 2012, where he has been working towards Ph. D. degree. His research interests include modeling and control of in-wheel vehicle.

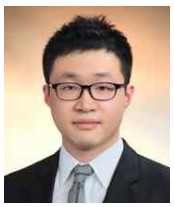

Ji-Weon Ko received B.S in mechanical engineering from Sungkyunkwan University, Suwon, Korea, in 2009, where he has been working towards Ph. D. degree. His research interests include modeling of electronic brake system and control of regenerative braking for hybrid electric vehicle and fuel cell electric vehicle

Sang-Moon Lee received M.S in mechanical engineering from Sungkyunkwan University, Suwon, Korea, in 2004. He has been working at MOBIS since 2010 in advanced development of in-wheel motor systems.

Jae-Seung Cheon received his Ph.D. degree in mechanical engineering from the Korea Advanced Institute of Science and Technology (KAIST) in 2003. He has been working at MOBIS since 2004 in advanced development of braking systems and in-wheel motor systems and is currently the head of the X-by-Wire Engineering team.

Hyun-Soo Kim received a Ph.D. degree in mechanical engineering from the University of Texas at Austin, Texas, USA, in 1986. Since 1986, he has worked as a Professor, Chairman, and Dean of the College of Engineering at Sungkyunkwan University. His main research interests include Hybrid Electric Vehicle (HEV) transmission system design, regenerative braking, and optimal power-distribution algorithms for HEV and vehicle stability control for In-wheel Electric Vehicles. He has authored numerous journal papers and patents. Prof. Kim served as a President of Electric Drive Vehicle Division of the Korea Society of Automotive Engineers and an editor of the International Journal of Automotive Technology.